Journal of Sound and Vibration 642 (2026) 119945

Contents lists available at ScienceDirect

Journal of Sound and Vibration

journal homepage: www.elsevier.com/locate/jsvi

Relevant features of intentional mistuning in forced response reduction: Application to centrifugal impellers

Giulio Deiana [a], Javier González-Monge [b,c,*], Carlos Martel [b,c], Alberto Guglielmo [d], Giulio Costa [d], Enrico Meli [a]

[a] Department of Industrial Engineering, University of Florence, Via S.Marta, 3, 50139, Florence, Italy
[b] Universidad Politécnica de Madrid, ETSI Aeronáutica y del Espacio, Plaza del Cardenal Cisneros 3, 28040, Madrid, Spain
[c] Departamento de Matemática Aplicada a la Ingeniería Aeroespacial, Spain
[d] Baker Hughes Nuovo Pignone Tecnologie s.r.l., Via Felice Matteucci, 2, 50127, Florence, Italy

ARTICLE INFO

Keywords:
Centrifugal impeller
Forced response
Mistuning
Intentional mistuning
Asymptotic methods

ABSTRACT

Centrifugal impellers are subjected to periodic loads during operation, which can excite modes with localized tip motion, leading to high cycle fatigue and structural failure. Small mistuning, typically caused by wear or manufacturing variations, can significantly amplify the forced response. In this work, we use the Asymptotic Mistuning Model (AMM) to investigate intentional mistuning strategies to reduce this amplification. The AMM assumes that mistuning and damping are small perturbations of the tuned problem, and provides a reduced-order model involving only the active modes contributing to the response. We apply it to a detailed finite element model of an industrial centrifugal impeller, obtaining high accuracy with a drastically simplified system. For this structure, a random mistuning of 0.5% of the sector mass can lead to a 50% increase in response amplitude. The design of an effective intentional mistuning pattern to reduce this amplification is guided by the information of the relevant features in the problem given by the AMM: the modal coupling occurs through particular Fourier coefficients of the sector-to-sector mistuning distribution. With this insight, we show that alternating patterns, effective in bladed-disks, are not suitable here due to the different modal distribution of the impeller. Instead, sinusoidal mistuning patterns targeting the modes present in the response are more effective, reducing both amplification and sensitivity to random mistuning. This is achieved without the need to run costly optimization procedures over an exponentially large number of configurations, as the asymptotic model already identifies the relevant physical mechanisms.

1. Introduction

During operation, turbomachinery systems are subjected to external periodic loads, which can induce high vibration levels when the excitation approaches a structural resonance. This forced response amplification is a critical issue, as it can lead to high cycle fatigue and structural failure.

Many turbomachinery components, such as bladed-disks or centrifugal impellers, are composed of identical sectors arranged in a cyclic configuration (tuned). However, small geometric imperfections introduced during manufacturing break this cyclic symmetry.

* Corresponding author.
E-mail addresses: giulio.deiana@unifi.it (G. Deiana), javier.gonzalez.monge@upm.es (J. González-Monge), carlos.martel@upm.es (C. Martel), alberto.guglielmo@bakerhughes.com (A. Guglielmo), giulio.costa@bakerhughes.com (G. Costa), enrico.meli@unifi.it (E. Meli).

https://doi.org/10.1016/j.jsv.2026.119945
Received 8 June 2025; Received in revised form 27 February 2026; Accepted 4 June 2026
Available online 5 June 2026

Mistuning, although small, can cause significant amplification of the forced response. This phenomenon has received considerable attention in the turbomachinery community and has been extensively studied (see, for example, the review by Castanier and Pierre [1]).

The problem of forced response in mistuned systems using realistic finite element models (FEM) is challenging due to the random nature of mistuning. These structures typically contain millions of degrees of freedom (DOFs), making forced response analyses computationally expensive, even in the absence of nonlinear effects. To reduce this cost while retaining accuracy, several reduced-order models (ROMs) have been developed. A Component Mode Synthesis (CMS) approach for bladed-disks was introduced in [2,3], where the system is reduced using separate disk and blade modes. A CMS variant was introduced in the Component Mode Mistuning Reduction (CMM) model [4]. An alternative ROM can be built using a Subset of Nominal Modes (SNM), projecting the equations of motion onto a much lower-dimensional space [5]. These nominal modes are obtained from the tuned system, which can be computed more easily by exploiting the cyclic symmetry. Other strategies include the use of a proper orthogonal decomposition (POD) to perturb the tuned modes with geometric mistuning information, and construct alternative reduction bases [6,7].

The Fundamental Mistuning Model (FMM) was introduced in [8] to analyze the forced response of a single modal family in a bladed-disk configuration. This approach reduces the system by projecting the equations of motion onto the tuned modes of that family, which is typically well separated in frequency from the others in this type of assembly. The FMM was subsequently applied to mistuning identification from experimental data, exploiting the reduced number of governing equations [9,10].

A refinement of the FMM, the Asymptotic Mistuning Model (AMM), was introduced in [11]. In this framework, only the subset of modes that actively participates in the response is retained; these are referred to as active modes. The number of active modes depends on the relative magnitude of the mistuning level and the frequency spacing between neighboring modes. The AMM has been used to compute the forced response of mistuned systems and has been validated against detailed FEM models of bladed disks [12,13], demonstrating high accuracy at a substantially reduced computational cost. Moreover, this asymptotic approach provides physical insight into the modal coupling mechanisms induced by mistuning and yields an improved upper bound for the maximum mistuning amplification compared to the classical result by Whitehead [14,15].

For bladed disks, the mistuned response is usually analyzed in two main scenarios: (i) isolated modes within a modal family, and (ii) clustered modes within the same family, which typically occur in configurations with a very stiff disk. While the FMM retains the entire family, the AMM focuses either on a single isolated mode or on the flat portion of a clustered family. In the latter case, an additional assumption is commonly introduced, namely that the in-sector mode shapes of the clustered modes are identical [11].

The maximum forced response amplification due to mistuning has also been investigated using simplified single-degree-of-freedom (1-DOF) models [16] and more detailed reduced-order models [17–19], once the corresponding model coefficients are properly calibrated. Such simplified models provide a good approximation for a single modal family in a bladed disk, where the in-sector mode shapes associated with different nodal diameters are similar. This framework has also been adopted in single-DOF-per-sector models [20,21] to analyze the effect of purely harmonic mistuning and the resulting modal coupling. In particular, for small mistuning levels such that only the counter-rotating TWs k and $-k$ with identical frequency are coupled, it has been shown that a harmonic mistuning with circumferential wavenumber $2k$ is required to couple these modes and split their frequencies [22,23].

For centrifugal impellers such as the one considered in this work, a different approach is required. These structures do not typically exhibit well-separated modal families, and neighboring modes in frequency can display significantly different in-sector mode shapes [24]. Moreover, the frequency spacing between modes with localized tip motion, critical due to fatigue damage, is often of the same order as the mistuning levels present in the structure. Consequently, coupling between modes with distinct in-sector mode shapes is expected, and it becomes necessary to investigate how to design effective intentional mistuning patterns under these conditions.

In the context of bladed disks, various intentional mistuning strategies have been proposed to mitigate forced response amplification induced by random mistuning. In [25], a prescribed mistuning pattern was shown to reduce mistuning sensitivity. Configurations employing two different blade types were investigated in [26,27], achieving a substantial reduction in vibration amplitude. Using the AMM, several studies have: clarified the mechanisms governing intentional mistuning [28]; designed simple alternating patterns with tip masses to suppress flutter [29,30]; and coupled modes with different aerodynamic characteristics to increase the overall damping for excitations with a given wavenumber [31]. The latter strategy relies on coupling the excited mode with another mode exhibiting higher aerodynamic damping, which can reduce the response below that of the tuned configuration. Similar objectives have also been achieved using other reduction techniques [32].

For centrifugal impellers, recent studies [33–35] have employed reduced-order models to analyze the forced response and design intentional mistuning patterns. In these works, an optimization procedure is used to identify the optimal mistuning configuration, leading to a number of evaluations that grows exponentially with the number of sectors. For example, $2^{12} = 4096$ configurations were analyzed in [35] using only two blade types in a 12-sector system. Such rapid growth of the design space can render the procedure computationally expensive when more complex mistuning patterns are considered. Additionally, Pettinato et al. [36] reported an experimental study using an SNM approach to identify mistuning characteristics for isolated modes within a single modal family. In [37], a CMM-based reduced-order model was developed to analyze the nonlinear forced response of mistuned centrifugal impellers with crack damage. More recently, Zhao et al. [38] combined experimental measurements and numerical simulations within a CMS framework to investigate blade vibrations in a mistuned industrial impeller of a single-stage centrifugal compressor.

In this work, for the first time we apply the AMM to study the forced response of a mistuned centrifugal impeller, rather than using more conventional reduced-order modeling strategies as described above. This approach provides a drastically reduced yet quantitatively accurate description of the problem. We employ this framework to analyze the amplification of the response and to design effective intentional mistuning patterns, emphasizing the differences with respect to other components such as bladed disks.

(a) Manufactured configuration

(b) Damaged centrifugal impeller (Picture from [39])

Fig. 1. Industrial centrifugal impeller (See Ref. [39]).

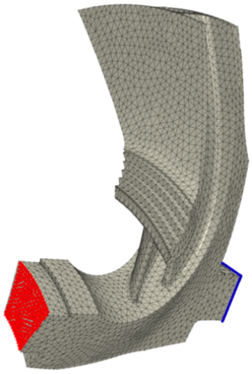

Fig. 2. Finite element model of one sector of the centrifugal impeller. The model contains $220,000$ DOFs and the complete impeller has $N = 13$ sectors. The front face (highlighted in red) is constrained only in the axial direction, while the rear face (highlighted in blue) is constrained in the plane orthogonal to the axial direction. (For interpretation of the references to colour in this figure legend, the reader is referred to the web version of this article.)

We consider an industrial centrifugal impeller similar to the configuration shown in Fig. 1a. Due to the stronger mechanical coupling between sectors, this type of impeller exhibits significantly higher natural frequencies than a typical bladed disk. Assessing mistuning sensitivity in this configuration is therefore of practical relevance, as damage has been observed in these structures for modes with localized motion near the blade tip (see Fig. 1b). Therefore, in contrast to bladed disks, the typical assumption that frequency-clustered modes share identical in-sector mode shapes is no longer valid, and the distinct mode shapes must be explicitly considered. We validate the AMM predictions against detailed FEM simulations of the full centrifugal impeller. The asymptotic model provides clear insight into the coupling mechanisms induced by mistuning, even when significantly different modes interact at a given mistuning level. The relevant components of the sector-to-sector mistuning distribution become apparent in the AMM equations, enabling the design of effective intentional mistuning patterns without resorting to computationally expensive optimization procedures, which constitutes one of the main advantages of the present approach.

The paper is structured as follows. We first introduce the centrifugal impeller that is analyzed, highlighting its differences from the more commonly studied bladed-disks configurations. Afterward, we review the mathematical formulation of the AMM. Next, we study the amplification in the response due to small random mistuning, and use the information of the asymptotic model to discuss and explain the most effective intentional mistuning strategies.

2. Model description

Centrifugal impellers are turbomachinery components used in pumps and compressors. They operate by accelerating the fluid radially outward, resulting in a pressure increase. The impeller typically consists of a set of blades attached to a central hub, with a shroud enclosing the outer diameter, as illustrated in Fig. 1a.

In operation conditions, the impeller is subjected to periodic loads. These excitations can induce high vibration levels, particularly when the forcing frequency is close to a structural resonance. To study the forced response problem, we consider a detailed FEM of

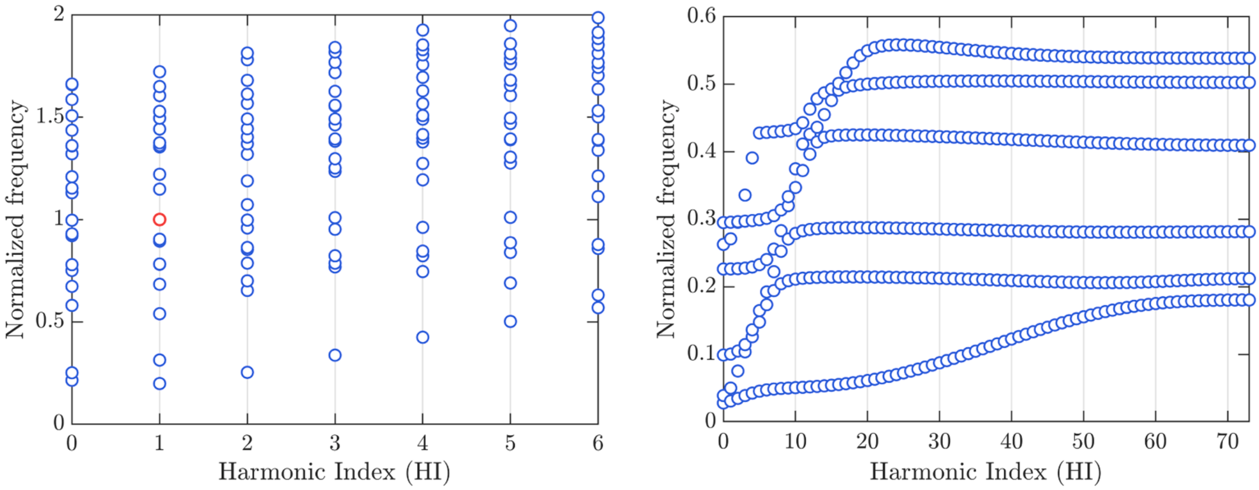

(a) Centrifugal impeller (b) Bladed-disk

Fig. 3. Modal frequencies as a function of the harmonic index.

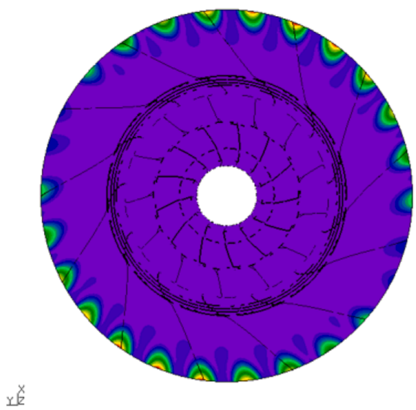

Fig. 4. Centrifugal impeller mode shape with HI 1 and localized motion at the tip (corresponding to the mode highlighted in red in Fig. 3a). (For interpretation of the references to colour in this figure legend, the reader is referred to the web version of this article.)

a single sector of the impeller, shown in Fig. 2. The model contains approximately $220,000$ DOFs and the complete impeller is made of $N = 13$ sectors.

A common way to represent the vibrational characteristics of turbomachinery structures is by plotting the natural frequencies as a function of the harmonic index (HI), or number of nodal diameters. For a tuned configuration (identical sectors), the natural frequencies of the centrifugal impeller are plotted in Fig. 3a (the negative HI are omitted since the frequencies are symmetric). Frequencies are normalized to protect proprietary data. For comparison, the frequencies of a bladed-disk are shown in Fig. 3b. The bladed-disk shows a clear separation between modal families, which are typically flat at high nodal diameters due to the small disk interaction between blades. In contrast, distinct families are not clearly visible in the centrifugal impeller; its frequencies are more densely clustered. This clustering has motivated recent efforts to develop modal tracking algorithms to identify similar mode shapes in such diagrams [24]. The impeller's natural frequencies are also higher than those of the bladed-disk, due to stronger inter-sector coupling.

For the reasons outlined in the previous paragraph, and given that flat modal families in bladed disks are typically analyzed under the assumption of identical in-sector mode shapes [11], we expect that common intentional mistuning strategies, such as alternating patterns [31], will not be effective for the centrifugal impeller. This will be demonstrated in the following sections.

The mode highlighted in red in Fig. 3a corresponds to a crossing in the interference diagram, also known as the SAFE (Singh's Advanced Frequency Evaluation) diagram [40] (speed lines not shown), and represents the main focus of the mistuning amplification analysis carried out in this work. This mode corresponds to a traveling wave (TW) with wavenumber 1, and its associated mode shape is shown in Fig. 4. The motion is localized at the tip of the sectors, and is critical for the forced response problem as it can lead to high cycle fatigue and failure of the structure (as illustrated in Fig. 1b). The external forcing analyzed throughout this work is a traveling wave with engine order 1 and a frequency close to this mode resonance.

3. Asymptotic mistuning model

To study the forced response of a mistuned centrifugal impeller, we use the Asymptotic Mistuning Model (AMM). This model assumes that mistuning and damping produce only small deviations from the tuned system, and it employs perturbation techniques to obtain a significantly reduced set of equations. In this section, we summarize the main aspects of the AMM to keep the paper self-contained; a more detailed derivation can be found in [11,13].

We begin by considering the tuned configuration of a centrifugal impeller with N sectors and m DOFs per sector. The full FEM equations for the forced oscillations are given by

$$\mathbf{M}_s\ddot{\mathbf{x}} + \mathbf{K}_s\mathbf{x} = \mathbf{f}(t), \tag{1}$$

where $\mathbf{M}_s$ and $\mathbf{K}_s$ are the mass and stiffness matrices of the entire assembly, respectively, $\mathbf{x}(t)$ is the vector of DOFs of the structure, and $\mathbf{f}(t)$ is the external forcing. The natural modes of vibration are obtained by setting $\mathbf{f}(t) = \mathbf{0}$, and assuming harmonic motion

$$\mathbf{x}(t) = \mathbf{X}e^{i\omega t} + \text{ c.c.}, \tag{2}$$

where c.c. denotes the complex conjugate. The vibration mode shape $\mathbf{X}$ and frequency ω are obtained by solving the generalized symmetric eigenvalue problem

$$\left(\mathbf{K}_s - \omega^2\mathbf{M}_s\right)\mathbf{X} = \mathbf{0}, \tag{3}$$

that can be expressed in terms of the in-sector matrices as

$$\left[\begin{pmatrix} \mathbf{K} & \mathbf{K}_c & \mathbf{0} & \cdots & \mathbf{K}_c^\top \\ \mathbf{K}_c^\top & \mathbf{K} & \mathbf{K}_c & \cdots & \mathbf{0} \\ \vdots & \vdots & \vdots & \ddots & \vdots \\ \mathbf{K}_c & \mathbf{0} & \cdots & \mathbf{K}_c^\top & \mathbf{K} \end{pmatrix} - \omega^2 \begin{pmatrix} \mathbf{M} & \mathbf{M}_c & \mathbf{0} & \cdots & \mathbf{M}_c^\top \\ \mathbf{M}_c^\top & \mathbf{M} & \mathbf{M}_c & \cdots & \mathbf{0} \\ \vdots & \vdots & \vdots & \ddots & \vdots \\ \mathbf{M}_c & \mathbf{0} & \cdots & \mathbf{M}_c^\top & \mathbf{M} \end{pmatrix}\right] \begin{pmatrix} \mathbf{X}_1 \\ \mathbf{X}_2 \\ \vdots \\ \mathbf{X}_N \end{pmatrix} = \begin{pmatrix} \mathbf{0} \\ \mathbf{0} \\ \vdots \\ \mathbf{0} \end{pmatrix}. \tag{4}$$

The vector $\mathbf{X}_j$ contains the displacements of the jth sector, the matrices $\mathbf{K}$ and $\mathbf{M}$ are the $m \times m$ in-sector stiffness and mass matrices, respectively, while $\mathbf{K}_c$ and $\mathbf{M}_c$ are the $m \times m$ coupling blocks between adjacent sectors. The cyclic symmetry is evident from Eq. (4), where the global matrices have a block circulant structure. This symmetry allows the eigenvectors to be expressed as

$$\begin{pmatrix} \mathbf{X}_1 \\ \mathbf{X}_2 \\ \vdots \\ \mathbf{X}_N \end{pmatrix} = \begin{pmatrix} \mathbf{Z}_k e^{i\left(\frac{2\pi k}{N}\right)0} \\ \mathbf{Z}_k e^{i\left(\frac{2\pi k}{N}\right)1} \\ \vdots \\ \mathbf{Z}_k e^{i\left(\frac{2\pi k}{N}\right)(N-1)} \end{pmatrix} \quad \text{for } k = 0, \dots, N-1, \tag{5}$$

which is just the sector-to-sector Discrete Fourier Transform (DFT) in the circumferential direction. The vector $\mathbf{Z}_k$ contains the in-sector mode shape for the kth harmonic index, and the displacements of the different sectors are just related by multiples of the interblade phase angle $2\pi/N$. The eigenvectors from Eq. (5) represent complex traveling wave modes with wavenumber k. Note that the mode with $N - k \equiv -k \pmod N$ is the traveling wave propagating in the opposite direction. A combination of these mode shapes can be used to represent the system in the so-called standing wave modes, although the traveling wave formulation is more convenient for the mistuning analysis.

Inserting Eq. (5) into Eq. (4) leads to N uncoupled eigenvalue problems of the size of one sector, m, given by

$$\left[\hat{\mathbf{K}}^k - \omega^2\hat{\mathbf{M}}^k\right]\mathbf{Z}_k = \mathbf{0}, \tag{6}$$

for $k = 0, \dots, N-1$. The matrices $\hat{\mathbf{K}}^k$ and $\hat{\mathbf{M}}^k$ are defined as

$$\begin{aligned} \hat{\mathbf{K}}^k &= \mathbf{K}_c^\top e^{-i\left(\frac{2\pi k}{N}\right)} + \mathbf{K} + \mathbf{K}_c e^{i\left(\frac{2\pi k}{N}\right)}, \\ \hat{\mathbf{M}}^k &= \mathbf{M}_c^\top e^{-i\left(\frac{2\pi k}{N}\right)} + \mathbf{M} + \mathbf{M}_c e^{i\left(\frac{2\pi k}{N}\right)}. \end{aligned} \tag{7}$$

For each k, there are m natural frequencies, $\omega_{k1}, \dots, \omega_{km}$, and complex eigenvectors, $\mathbf{Z}_{k1}, \dots, \mathbf{Z}_{km}$. The mode shapes can be arranged as columns in a matrix

$$\mathbf{P}_k = \begin{pmatrix} \mathbf{Z}_{k1} & \mathbf{Z}_{k2} & \cdots & \mathbf{Z}_{km} \end{pmatrix}, \tag{8}$$

which is normalized to satisfy

$$\begin{aligned} &\mathbf{P}_k^H\hat{\mathbf{M}}^k\mathbf{P}_k = \mathbf{I}, \\ &\mathbf{P}_k^H\hat{\mathbf{K}}^k\mathbf{P}_k = \boldsymbol{\Omega}_k^2 = \mathbf{diag}(\omega_{k1}^2, \dots, \omega_{km}^2), \end{aligned} \tag{9}$$

for $k = 0, \dots, N-1$, and the superscript H denotes the Hermitian transpose. With these matrices, a change of basis from physical displacements, $\mathbf{X}$, to the TW amplitudes, $\mathbf{A}$, can be defined

$$\mathbf{X} = \mathbf{P}\mathbf{A}, \tag{10}$$

where the matrix $\mathbf{P}$ is defined as

$$\mathbf{P} = \frac{1}{\sqrt{N}}\begin{pmatrix} \mathbf{P}_0 e^{i\left(\frac{2\pi 0}{N}\right)0} & \cdots & \mathbf{P}_{N-1} e^{i\left(\frac{2\pi(N-1)}{N}\right)0} \\ \vdots & \ddots & \vdots \\ \mathbf{P}_0 e^{i\left(\frac{2\pi 0}{N}\right)(N-1)} & \cdots & \mathbf{P}_{N-1} e^{i\left(\frac{2\pi(N-1)}{N}\right)(N-1)} \end{pmatrix}, \tag{11}$$

and

$$\mathbf{A} = \sqrt{N}\begin{pmatrix} \mathbf{A}_0 \\ \vdots \\ \mathbf{A}_{N-1} \end{pmatrix} \tag{12}$$

contains the amplitudes of all TW modes with wavenumber $k = 0, \dots, N-1$.

Going back to the forced response problem (1), we consider that the external forcing has the form of a traveling wave with engine order r and frequency ω

$$\mathbf{f}(t) = \mathbf{F}_s e^{i\omega t} + \text{ c.c.} = \begin{pmatrix} \mathbf{F} e^{i\left(\frac{2\pi r}{N}\right)0} \\ \vdots \\ \mathbf{F} e^{i\left(\frac{2\pi r}{N}\right)(N-1)} \end{pmatrix} e^{i\omega t} + \text{ c.c.} \tag{13}$$

Assuming that the response is also harmonic, the forced response problem of the tuned system is reduced to the linear system

$$\left(\mathbf{K}_s - \omega^2 \mathbf{M}_s\right)\mathbf{X} = \mathbf{F}_s. \tag{14}$$

This problem takes a diagonal form in the traveling wave basis, obtained by using (10) and premultiplying by $\mathbf{P}^H$, resulting in

$$\begin{pmatrix} \boldsymbol{\Omega}_0^2 - \omega^2\mathbf{I} & \cdots & \mathbf{0} \\ \vdots & \ddots & \vdots \\ \mathbf{0} & \cdots & \boldsymbol{\Omega}_{N-1}^2 - \omega^2\mathbf{I} \end{pmatrix}\begin{pmatrix} \mathbf{A}_0 \\ \vdots \\ \mathbf{A}_{N-1} \end{pmatrix} = \begin{pmatrix} \mathbf{0} \\ \vdots \\ \mathbf{P}_r^H\mathbf{F} \\ \vdots \\ \mathbf{0} \end{pmatrix}. \tag{15}$$

Therefore, in the tuned system, only the TW components $\mathbf{A}_r$ are different from zero, since the forcing is only present in the rth block in the TW basis.

Including now the effect of mistuning and damping, the forced response problem takes the form

$$\left((1 + i\delta)\mathbf{K}_s + \Delta\mathbf{K}_s - \omega^2(\mathbf{M}_s + \Delta\mathbf{M}_s)\right)\mathbf{X} = \mathbf{F}_s, \tag{16}$$

where the damping is modeled as proportional to the stiffness matrix. The parameter δ is small ($\delta \ll 1$), representing a realistic value. The mistuning matrices are defined as

$$\Delta\mathbf{K}_s = \begin{pmatrix} \Delta\mathbf{K}_1 & \mathbf{0} & \cdots & \mathbf{0} \\ \mathbf{0} & \Delta\mathbf{K}_2 & \cdots & \mathbf{0} \\ \vdots & \vdots & \ddots & \vdots \\ \mathbf{0} & \mathbf{0} & \cdots & \Delta\mathbf{K}_N \end{pmatrix}, \quad \Delta\mathbf{M}_s = \begin{pmatrix} \Delta\mathbf{M}_1 & \mathbf{0} & \cdots & \mathbf{0} \\ \mathbf{0} & \Delta\mathbf{M}_2 & \cdots & \mathbf{0} \\ \vdots & \vdots & \ddots & \vdots \\ \mathbf{0} & \mathbf{0} & \cdots & \Delta\mathbf{M}_N \end{pmatrix}, \tag{17}$$

where no mistuning is introduced in the coupling between sectors, as these DOFs represent a much smaller subset compared to the in-sector DOFs. The in-sector matrices are symmetric, and satisfy

$$\sum_{j=1}^{N} \Delta\mathbf{K}_j = 0, \quad \sum_{j=1}^{N} \Delta\mathbf{M}_j = 0, \tag{18}$$

which implies that the average mistuning across all sectors is zero. This is equivalent to assuming that the mean component of the mistuning is included in the tuned system without loss of generality.

The forced response problem of the structure with mistuning (16) expressed in the TW basis takes the form

$$\left[\begin{pmatrix} (1+i\delta)\boldsymbol{\Omega}_0^2 - \omega^2\mathbf{I} & \cdots & \mathbf{0} \\ \vdots & \ddots & \vdots \\ \mathbf{0} & \cdots & (1+i\delta)\boldsymbol{\Omega}_{N-1}^2 - \omega^2\mathbf{I} \end{pmatrix} + \boldsymbol{\Delta}\right]\begin{pmatrix} \mathbf{A}_0 \\ \vdots \\ \mathbf{A}_{N-1} \end{pmatrix} = \begin{pmatrix} \mathbf{0} \\ \vdots \\ \mathbf{P}_r^H\mathbf{F} \\ \vdots \\ \mathbf{0} \end{pmatrix}, \tag{19}$$

and the matrix $\boldsymbol{\Delta}$ is given by

$$\boldsymbol{\Delta} = \mathbf{P}^H\left(\Delta\mathbf{K}_s - \omega^2\Delta\mathbf{M}_s\right)\mathbf{P}, \tag{20}$$

where $\mathbf{P}$ is the transformation matrix that relates the displacement basis to the TW basis defined in Eq. (11). The matrix $\boldsymbol{\Delta}$ can be simplified using the orthogonality properties of the DFT. First, the in-sector mistuning matrices are expressed in terms of their spatial Fourier coefficients as

$$\Delta\mathbf{K}_j = \sum_{k=0}^{N-1} \Delta\mathbf{K}_k^F e^{i\left(\frac{2\pi k}{N}\right)j}, \quad \Delta\mathbf{M}_j = \sum_{k=0}^{N-1} \Delta\mathbf{M}_k^F e^{i\left(\frac{2\pi k}{N}\right)j}, \tag{21}$$

for $j = 1, \ldots, N$. Inserting these expressions into the definition of $\mathbf{\Delta}$ and using Eq. (5), the mistuning matrix in the TW basis takes the form

$$\mathbf{\Delta} = \begin{pmatrix} \mathbf{0} & \mathbf{\Delta}_{0,1} & \cdots & \mathbf{\Delta}_{0,N-1} \\ \mathbf{\Delta}_{1,0} & \mathbf{0} & \cdots & \mathbf{\Delta}_{1,N-1} \\ \vdots & \vdots & \ddots & \vdots \\ \mathbf{\Delta}_{N-1,0} & \mathbf{\Delta}_{N-1,1} & \cdots & \mathbf{0} \end{pmatrix}, \tag{22}$$

where each block $\mathbf{\Delta}_{k,n}$ is given by

$$\mathbf{\Delta}_{k,n} = \mathbf{P}_k^H (\Delta \mathbf{K}_{k-n}^F - \omega^2 \Delta \mathbf{M}_{k-n}^F) \mathbf{P}_n. \tag{23}$$

The coupling between different TW modes is only produced by the mistuning matrix, which is non-diagonal in this basis. Moreover, the coupling between modes k and n occurs through the $k - n$ Fourier coefficient of the mistuning matrices.

We now introduce the AMM equations to study the response in the vicinity of a tuned resonant frequency of interest, ω_{tun}. The external forcing has the shape of a TW with the same wavenumber as the mode associated to this frequency. For small damping and mistuning, a drastic reduction can be performed, retaining only a small set of active modes-those expected to contribute significantly to the response. Under this assumption, the AMM equations take the form

$$\begin{pmatrix} d_k & D_{k,k-1} & \cdots & D_{k,-k} \\ \bar{D}_{k,k-1} & d_{k-1} & \cdots & D_{k-1,-k} \\ \vdots & \vdots & \ddots & \vdots \\ \bar{D}_{k,-k} & \bar{D}_{k-1,-k} & \cdots & d_{-k} \end{pmatrix} \begin{pmatrix} A_k \\ A_{k-1} \\ \vdots \\ A_{-(k-1)} \\ A_{-k} \end{pmatrix} = \begin{pmatrix} 0 \\ \vdots \\ i\delta\omega_{\text{tun}}/2 \\ \vdots \\ 0 \end{pmatrix}, \tag{24}$$

where $A_k, \ldots, A_{-k}$ are the amplitudes of the active TW modes, ordered to distinguish between forward and backward TWs. The diagonal elements d_k are defined as

$$d_k = \Delta\omega_k - \Delta\omega + i\delta\omega_{\text{tun}}/2, \tag{25}$$

where $\Delta\omega_k = \omega_k - \omega_{\text{tun}}$ is the difference between the tuned frequency ω_k of mode A_k and the reference resonant frequency ω_{tun}. The term $\Delta\omega = \omega - \omega_{\text{tun}}$ represents the offset between the forcing frequency and tuned resonance.

The off-diagonal elements $D_{k,n}$ are computed from the projection of the Fourier coefficients of the mistuning matrices onto the corresponding tuned modes

$$D_{k,n} = \mathbf{Z}_k^H \left(\Delta \mathbf{K}_{k-n}^F - \omega_{\text{tun}}^2 \Delta \mathbf{M}_{k-n}^F\right) \mathbf{Z}_n / (2\omega_{\text{tun}}), \tag{26}$$

and $\bar{D}_{k,n}$ denotes the complex conjugate. These off-diagonal terms govern the coupling between modes. They are independent of the forcing frequency due to the approximation in the AMM $\omega = \omega_{\text{tun}} + \Delta\omega$ (where $\Delta\omega \ll 1$), which is valid close to the resonance crossing.

Therefore, given the mistuning distribution and the tuned modes and frequencies, the AMM system can be fully assembled and solved. The value of the forcing in the right-hand side, $i\delta\omega_{\text{tun}}/2$, is chosen such that the tuned response for a forcing with engine order r is normalized: $A_r = 1$ and $A_k = 0$ for $k \neq r$.

The number of active modes required in the AMM depends on the relative magnitude of mistuning and damping compared to the spacing of the modal frequencies. For very small mistuning, only modes k and $-k$ are coupled (since their tuned frequencies are exactly the same), and the response can be accurately captured by a 2×2 system. As mistuning increases, additional modes must be included. Typically, the number of retained modes for a fixed level of mistuning is increased until the solution converges.

A final remark concerning the AMM is that, apart from computing the forced response, the mistuned frequencies and mode shapes can be obtained by formulating the left-hand side of Eq. (24) as an eigenvalue problem, where the eigenvalue is $\Delta\omega$, as defined through the diagonal terms d_k in Eq. (25). The corresponding mistuned mode shapes are given, to the order of approximation of the AMM, by the linear combination of tuned active TW modes determined by the mistuning distribution.

4. Forced response analysis

We now use the AMM to compute the forced response of the centrifugal impeller with mistuning. While we focus on the centrifugal impeller presented in Fig. 2, the AMM methodology can also be applied to other turbomachinery components by following the procedure described in Section 3.

The damping is set to $\delta = 0.1\%$, consistent with typical values observed in such structures. To validate the asymptotic approach for this industrial case, we consider an additional mass placed at the tip of each sector, as shown in Fig. 5. For the jth sector, this mass defines the term $\Delta \mathbf{M}_j$ in the mistuning matrix, and stiffness mistuning is neglected $\Delta \mathbf{K}_s = \mathbf{0}$. In general, stiffness mistuning can be incorporated as described in Eq. (26), which would introduce an additional contribution to the elements of the mistuning matrix.

The mistuning of the different sectors is parametrized with a single matrix, $\Delta \mathbf{M}$, corresponding to the DOFs highlighted in red in Fig. 5. Then, the sector-to-sector mistuning distribution is described by the parameter ε_j,

$$\Delta \mathbf{M}_j = \varepsilon_j \Delta \mathbf{M}, \quad \text{for } j = 1, \ldots, N. \tag{27}$$

To construct the AMM equations, we define three frequency bands around the mode of interest, which is highlighted in red in Fig. 3a. A zoomed-in view of the surrounding frequencies is shown in Fig. 6. The first band contains five active modes (only three are

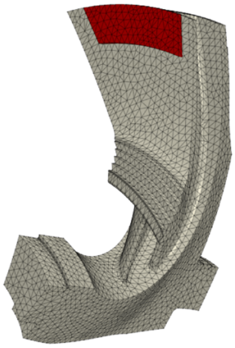

Fig. 5. Definition of the size and placement of the intentional mistuning mass in each sector.

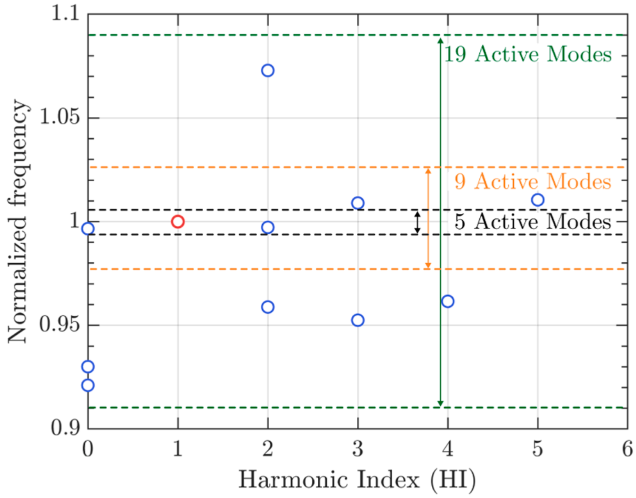

Fig. 6. Frequency bands containing the different active modes used in the asymptotic model.

visible in the plot, but the symmetric counterparts of $k = 1, 2$, $k = -1, -2$, are also included, since they have the same frequency). An intermediate band includes 9 active modes, and a larger band comprises 19 active modes, covering up to $\pm 10\%$ relative frequency deviation from the forced mode.

These three AMM models are used to validate the asymptotic approach against the full-order system. To facilitate understanding in the construction of the AMM, the system with five active modes is explicitly shown below

$$\begin{pmatrix} d_2 & D_{2,1} & D_{2,0} & D_{2,-1} & D_{2,-2} \\ & d_1 & D_{1,0} & D_{1,-1} & D_{1,-2} \\ & & d_0 & D_{0,-1} & D_{0,-2} \\ & \text{h.c.} & & d_{-1} & D_{-1,-2} \\ & & & & d_{-2} \end{pmatrix} \begin{pmatrix} A_2 \\ A_1 \\ A_0 \\ A_{-1} \\ A_{-2} \end{pmatrix} = \begin{pmatrix} 0 \\ i\delta\omega_{\text{tun}}/2 \\ 0 \\ 0 \\ 0 \end{pmatrix}, \tag{28}$$

where the lower triangular part is the Hermitian conjugate of the upper part. Among the five modes involved in the response, only TW0 lacks a counterrotating counterpart, as its associated mode shape is purely real with all sectors moving in phase. The external forcing appears only in the TW1 equation, since this is the mode excited that is related to dangerous localized tip motion.

4.1. Validation of the AMM

To validate the AMM model, we consider three mistuning patterns with 2% amplitude:

(i) $\varepsilon_j = 0.02 \cdot \text{ rand}(j)$
(ii) $\varepsilon_j = 0.02 \cdot \cos\left((2\pi/N \cdot 1)(j-1)\right)$
(iii) $\varepsilon_j = 0.02 \cdot \cos\left((2\pi/N \cdot 3)(j-1)\right)$

The three AMM systems described above are solved and compared with the full-order FEM solution of Eq. (16). The complete model consists of approximately 3 million complex linear equations and is solved directly using the Pardiso library [41]. On a workstation

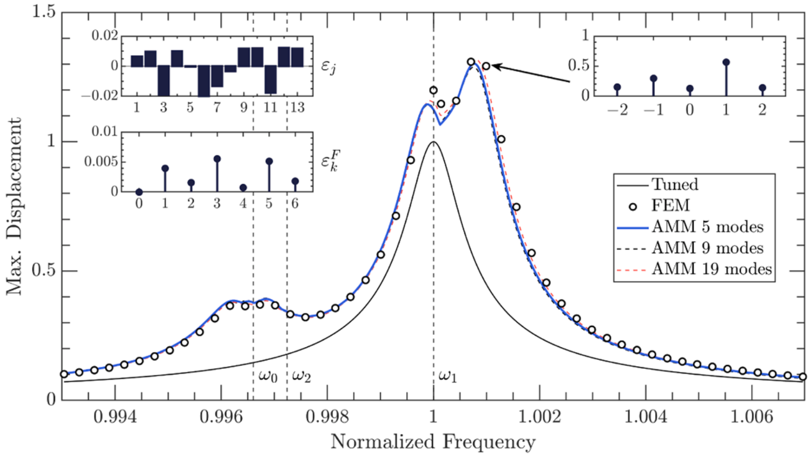

(a) Random mistuning pattern, $\varepsilon_j = 0.02 \cdot \text{ rand}(j)$

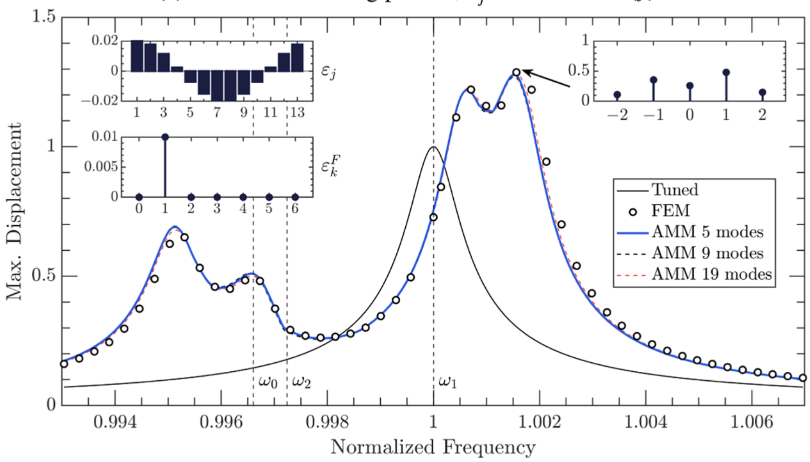

(b) Cosine pattern with wavenumber 1, $\varepsilon_j = 0.02 \cdot \cos((2\pi/N \cdot 1)(j-1))$

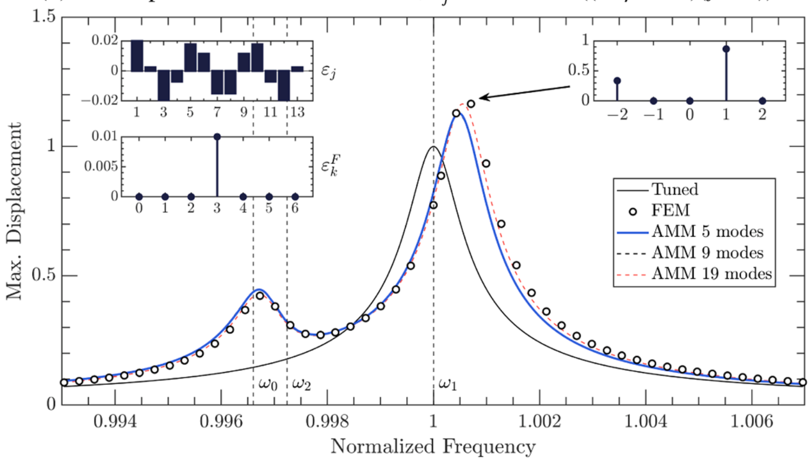

(c) Cosine pattern with wavenumber 3, $\varepsilon_j = 0.02 \cdot \cos((2\pi/N \cdot 3)(j-1))$

Fig. 7. Frequency response curve of the maximum displacement over all the sectors. Comparison between the AMM with different levels of approximation (blue line and dashed colored lines) and the full-order FEM solution (dots). The tuned response is included as a reference (black thin line), with the frequencies of the tuned modes ω_0, ω_1 and ω_2 indicated by the vertical dashed lines. Top left: mistuning pattern in physical space (ε_j), and in Fourier space (ε_k^F). Top right: Modal amplitudes of the traveling waves $-2, -1, 0, 1, 2$. (For interpretation of the references to colour in this figure legend, the reader is referred to the web version of this article.)

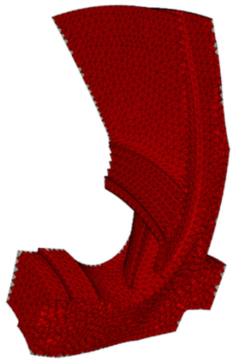

Fig. 8. Representation of the in-sector random mistuning.

equipped with an Intel® Core™i9-13900K (3.00 GHz, 24 cores, 32 threads) and 128 GB of RAM, each linear system requires about 15 min of CPU time. The computational cost of solving the AMM is negligible.

The results are shown in Fig. 7, where frequency response curves are plotted using the maximum displacement across all sectors. In Fig. 7a, the response for the random mistuning pattern in (i) is presented. The tuned response is included as a reference (thin black line), and the tuned frequencies of modes 0, 1, and 2 from the first frequency band in Fig. 6 are marked with vertical dashed lines and labeled ω_0, ω_1, and ω_2. The mistuning distribution ε_j is shown in the top left, along with its spatial Fourier transform ε_k^F, which is important to understand the coupling in the AMM framework. The 5-mode AMM solution is plotted in blue, while the 9- and 19-mode approximations are shown with dashed black and red lines, respectively. The full FEM response is marked with white dots. As shown, the AMM captures the forced response accurately even with only 5 active modes. The maximum deviation from the FEM solution occurs near the resonance peak, with a discrepancy of less than 3%.

The modal content at resonance is shown in the top right of the figure. The TWs 1 and −1 dominate the response, with additional contributions from TWs 0, 2, and −2. Other components are omitted for clarity due to their negligible contribution. The strong presence of TWs 1 and −1 is expected, as they share the same tuned frequency and are easily coupled by mistuning.

Fig. 7b shows the frequency response for the cosine mistuning pattern with wavenumber one (case (ii)). As shown in the top left, this distribution contains only one non-zero Fourier coefficient. The AMM again closely matches the FEM solution. Near resonance, the response involves several modes that are coupled through mistuning.

The response for the cosine pattern with wavenumber three (case (iii)) is shown in Fig. 7c, again demonstrating good agreement with the FEM solution. In this case, the dominant contribution at the resonance peak comes from TWs 1 and −2. This behavior is consistent with the presence of the Fourier coefficient ε_3^F, which, according to the AMM formulation, couples modes separated by three in harmonic index (see the definition of $D_{k,n}$ in Eq. (26)).

Given the accuracy of the asymptotic approximation, we now restrict our analysis to the reduced AMM system to study the sensitivity of the centrifugal impeller to random mistuning and to explore effective strategies for intentional mistuning.

4.2. *Amplification by random mistuning*

To model the random mistuning arising from geometric imperfections, we consider an in-sector distribution, as illustrated in Fig. 8. The mistuning amplitude is set to 0.5% of the sector mass.

The amplification caused by random mistuning is evaluated by generating 100 different random patterns. The corresponding resonance curves are plotted in Fig. 9, with each individual response shown in blue. The thick red line highlights the case with the maximum amplification, showing an increase of approximately 48% in the peak response compared to the tuned case. This is a considerable amplification given the small mistuning level.

On the left side of the figure, the mistuning distribution for this case is shown. Its Fourier decomposition indicates that the $k = 1$ component has the highest amplitude. According to the AMM formulation, this component couples neighboring modes (those separated by one in harmonic index). As expected, the modal amplitudes at the peak show contributions from modes $0, 1, -1, 2$, and -2.

The displacements of the nodes of the centrifugal impeller at the peak of the resonance curve with the highest amplification are shown in Fig. 10. Their reconstruction using the AMM with only five active modes is presented in Fig. 10a, while the full FEM solution is given in Fig. 10b. This comparison provides an additional validation of the AMM, as the structural deformation is very similar, accurately reproducing the real displacement field.

4.3. *Intentional mistuning*

The design of an effective mistuning pattern requires separating the frequencies between the dominant modes in the response, in order to reduce the peak amplitude. Intentional mistuning is applied, on top of the random in-sector pattern used in the response of Fig. 9, using the same tip masses described in Fig. 5.

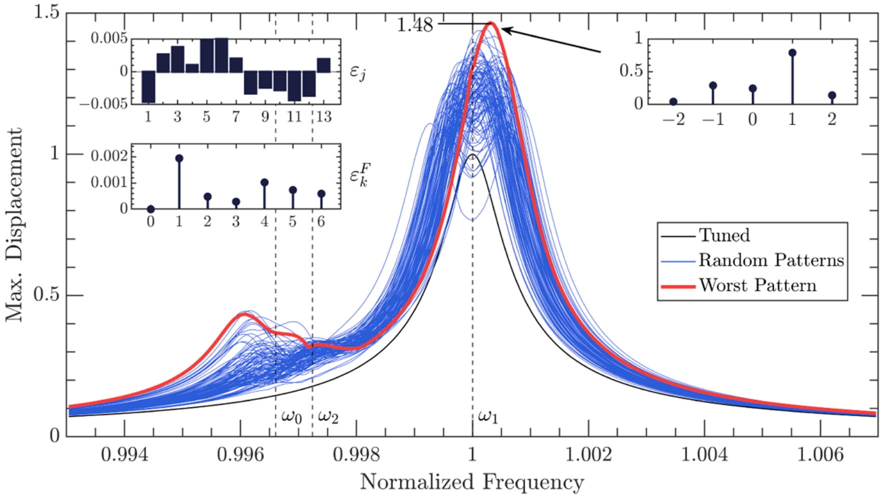

Fig. 9. Frequency response curve of the maximum displacement over all the sectors of 100 different random mistuning patterns with 0.5% amplitude. The mistuning pattern with the largest amplification is highlighted with thick red line. Top left: mistuning pattern producing the largest amplification in physical space (ε_j), and in Fourier space (ε_k^F). Top right: Modal amplitudes of the traveling waves $-2, -1, 0, 1, 2$ at the peak. (For interpretation of the references to colour in this figure legend, the reader is referred to the web version of this article.)

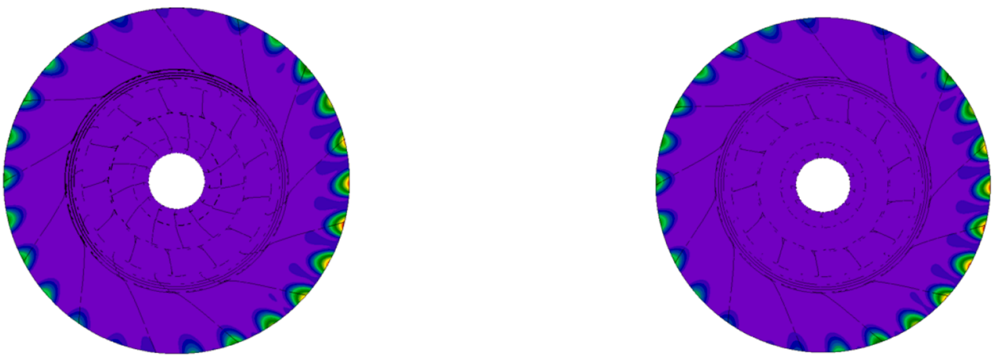

(a) AMM, 5 active modes

(b) FEM solution

Fig. 10. Comparison between the displacement field of the forced response reconstructed using the AMM and the full FEM solution at the resonance peak of the random mistuning case (Fig. 9).

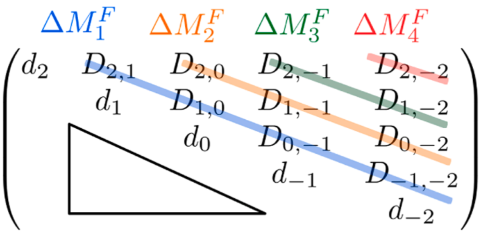

Fig. 11. Detailed view of the effect of the different Fourier components of the mistuning matrix in the coupling of the active modes of the response.

From the TW components at the peak in the random pattern in Fig. 9, we know that the response is primarily composed of five modes within a narrow frequency band around the excited one. To determine which mistuning patterns are more effective and guide the design, we examine the relevant Fourier components of the mistuning matrices in the AMM equations, as depicted in Fig. 11.

The coupling between TW 1 and -1 is controlled by the term $D_{1,-1}$, which depends only on the Fourier coefficient $\Delta\mathbf{M}_2^F$. Thus, a mistuning pattern containing only this component is expected to separate these two modes, reducing the response. Similarly, to decouple TWs 1 and -1 from modes 0, 2, and -2, a pattern with a strong $\Delta\mathbf{M}_1^F$ component is effective, since this coefficient appears in the associated coupling terms. In contrast, a pattern with $\Delta\mathbf{M}_3^F$ only weakly affects the interaction between modes 1, -1, and 2, -2 and does not interact with TW 0. The impact of $\Delta\mathbf{M}_4^F$ is expected to be negligible, as it only affects the coupling between modes 2

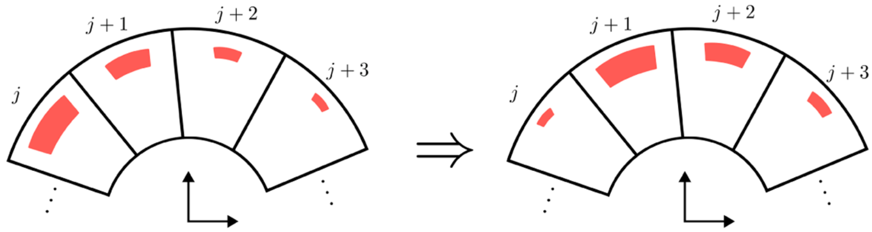

Fig. 12. Difference in placement of a specific mistuning pattern.

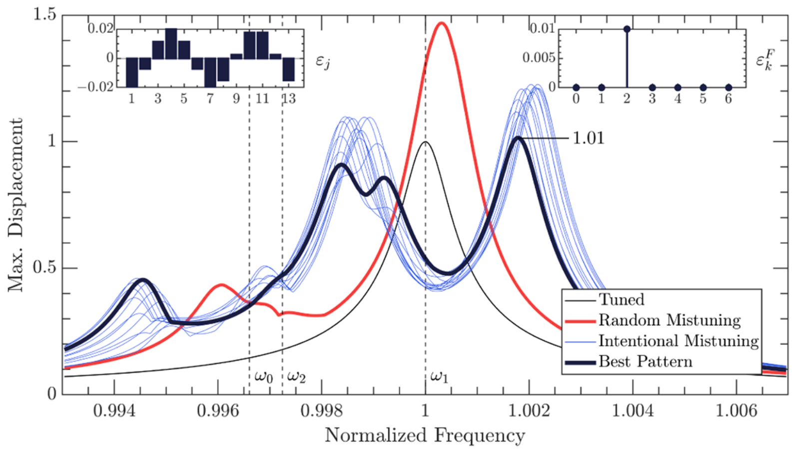

Fig. 13. Frequency response curve of the maximum displacement over all the sectors. Effect of the phase of the intentional mistuning pattern, $\varepsilon_j = 0.02 \cdot \cos((2\pi/N \cdot 2)(j-1) + (2\pi/N)\ell)$, for different ℓ. The lowest response is obtained for $\ell = 7$ (thick black line). Top left: intentional mistuning pattern with highest reduction in physical space (ε_j). Top right: intentional mistuning pattern with highest reduction in Fourier space (ε_k^F).

and −2. Additionally, the alternating mistuning pattern, commonly effective in bladed-disks due to their flat modal families, is also evaluated here.

Based on this analysis, the following intentional mistuning patterns are considered:

(a) Cosine pattern with wavenumber 2
(b) Cosine pattern with wavenumber 1
(c) Cosine pattern with wavenumber 3
(d) Cosine pattern with wavenumber 4
(e) Alternating pattern

The effect of each mistuning pattern is evaluated for different amplitudes and phase shifts along the impeller. This sensitivity to placement is illustrated in Fig. 12. Since the underlying mistuning of each blade is unique, shifting a given pattern can alter its interaction with the underlying imperfections. With only 13 sectors, this discrete effect becomes significant, and different phase shifts (corresponding to multiples of the interblade phase angle) are studied in terms of the amplification reduction they produce.

(a) Cosine pattern with wavenumber 2

The intentional mistuning pattern is given by

$$\varepsilon_j \sim \cos((2\pi/N \cdot 2)(j-1) + (2\pi/N)\ell), \tag{29}$$

for $j = 1, \ldots, N$, and ℓ is an integer parameter used to study the effect of shifting the mistuning pattern along the impeller. The amplitude of the intentional mistuning pattern is fixed at 2%, and is applied on top of the random mistuning distribution that produced nearly 50% amplification (see Fig. 9). The frequency response curves for different values of ℓ are shown in Fig. 13, with the response of the system without intentional mistuning included in red for reference. In all cases, the intentional mistuning leads to a significant reduction in amplification, reaching approximately 20% of the tuned response. The configuration with $\ell = 7$, highlighted in black, provides the lowest peak amplitude (only 1% above the tuned case). Its corresponding mistuning distribution is shown in the top left, and the top right plot shows a single peak, since it is a pure wavenumber 2 cosine pattern.

Next, we fix $\ell = 7$ and vary the amplitude of the intentional mistuning from 0% to 5%. The resulting frequency responses are shown in Fig. 14. For small mistuning levels (0.5-1%), the frequency separation between TW 1 and −1 is minor, resulting in only a mild reduction. The minimum amplification occurs at 2%, and further increasing the amplitude leads to a rise in peak response. This

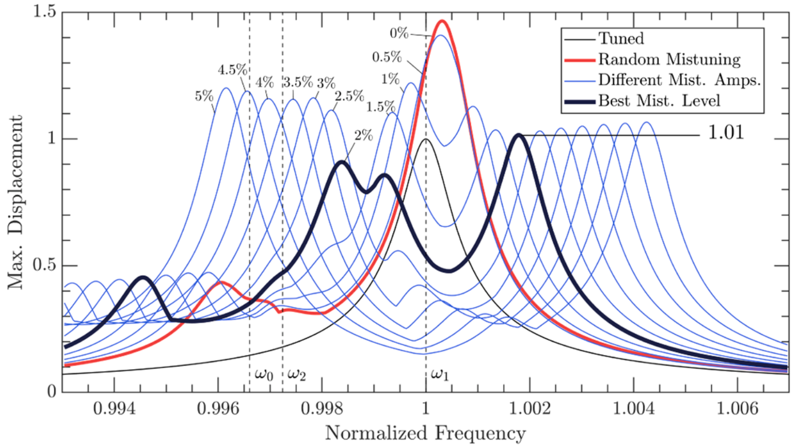

Fig. 14. Frequency response curve of the maximum displacements over all the sectors for different intentional mistuning amplitudes for the cosine pattern with wavenumber 2.

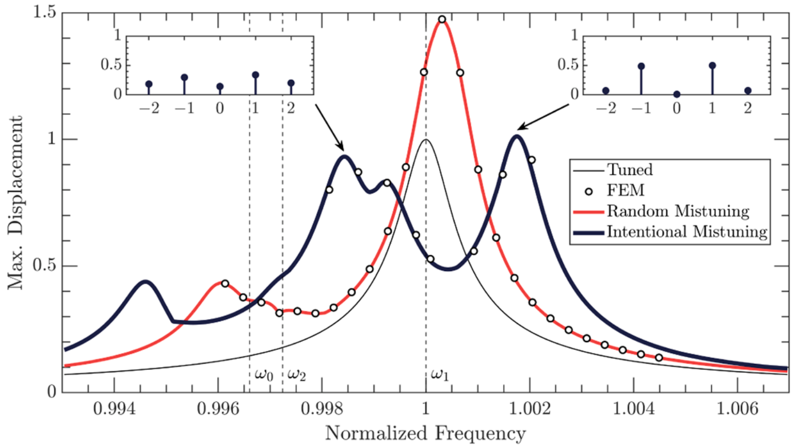

Fig. 15. Validation of the resonance curve with the intentional mistuning pattern comparing the AMM prediction (lines) against full-order FEM calculation (dots). Inset plots: Modal amplitudes of the traveling waves $-2, -1, 0, 1, 2$, at the two peaks.

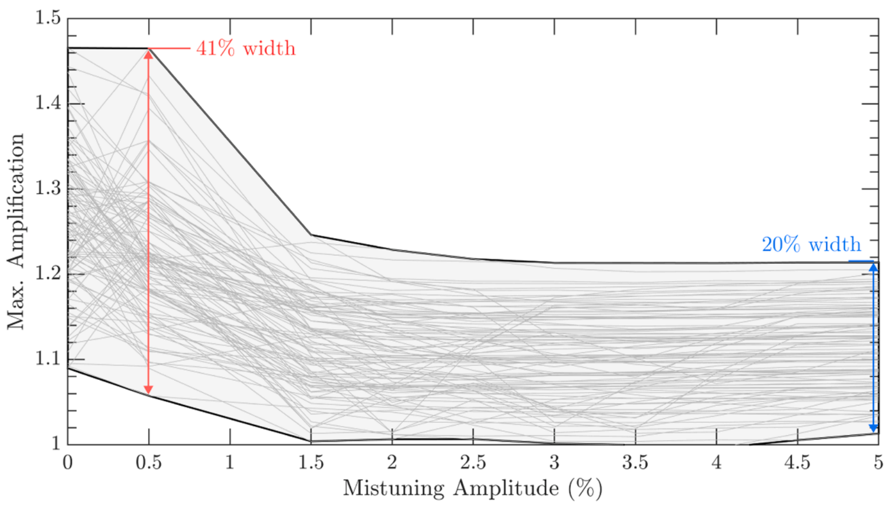

Fig. 16. Maximum amplification of all the random mistuning patterns in Fig. 9 for an intentional mistuning pattern with a cosine distribution of wavenumber 2.

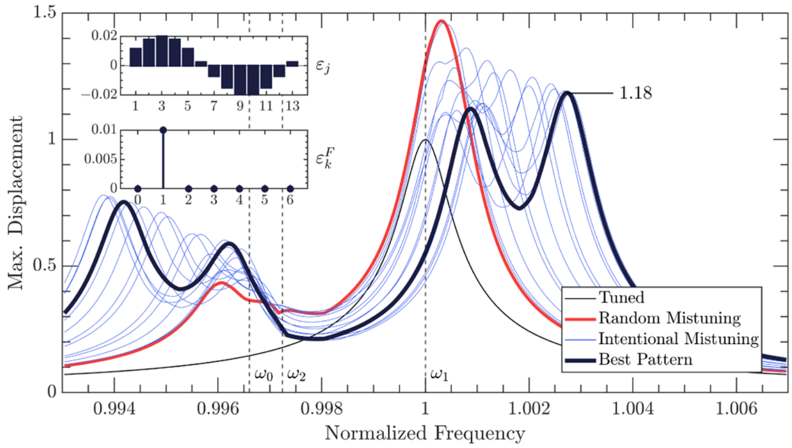

Fig. 17. Frequency response curve of the maximum displacement over all the sectors. Effect of the phase of the intentional mistuning pattern, $\varepsilon_j = 0.02 \cdot \cos((2\pi/N \cdot 1)(j-1) + (2\pi/N)\ell)$, for different ℓ. The lowest response is obtained for $\ell = 11$ (thick black line). Top left: intentional mistuning pattern with the highest reduction in physical space (ε_j), and in Fourier space (ε_k^F).

is due to TW -1 shifting closer to TWs 0, 2, and -2, causing additional coupling and higher amplification. Although the peak remains significantly below the level observed without intentional mistuning, this effect highlights the importance of nearby mode placement. In centrifugal impellers, where the modal density is higher than in bladed-disks, large mistuning amplitudes may unintentionally introduce new couplings and limit the effectiveness of the strategy.

As an additional validation of the AMM, the resonance curves for the random pattern with high amplification and the intentional pattern with the lowest response are compared against full FEM simulations in Fig. 15. Excellent agreement is observed. The inset plots show the modal content of the two peaks after the separation induced by the mistuning. The right peak is dominated by TWs 1 and -1, with negligible contributions from other modes. Notably, the amplitude of TW 1 is smaller than in the random pattern case. The left peak shows participation of all five dominant modes, although with relatively low amplitude.

Up to this point, the analysis focused on the specific random pattern that produced the highest amplification. To assess the general effectiveness of the intentional mistuning pattern, we now apply it to all 100 random distributions used in Fig. 9. The maximum amplification for each case is shown in Fig. 16 as a function of the intentional mistuning amplitude. For low levels of mistuning, the amplification varies significantly, with a spread of 41% between the random cases. As the intentional mistuning increases, the peak amplification drops rapidly to around 1.2. However, at higher mistuning levels (around 5%), the variation remains large. This is consistent with earlier observations: increasing the amplitude too much brings the mistuned frequency of TW -1 closer to other modes, introducing additional interactions and limiting sensitivity reduction to random mistuning.

(b) Cosine pattern with wavenumber 1

In this case, the intentional mistuning is defined according to the distribution

$$\varepsilon_j \sim \cos((2\pi/N \cdot 1)(j-1) + (2\pi/N)\ell). \tag{30}$$

We begin by setting the amplitude of the intentional mistuning to 2% and analyzing the effect of shifting the pattern through the parameter ℓ. The corresponding resonance curves are shown in Fig. 17. As predicted by the AMM, a wavenumber 1 mistuning distribution promotes coupling that pushes the modes apart. As a result, the peak near the tuned frequency ω_1 splits into two distinct peaks that shift toward higher frequencies, while the resonances associated with modes 0 and 2 move left. The influence of ℓ is again noticeable: some shifts provide limited reduction in amplitude, while others are more effective. The best result is obtained for $\ell = 11$, highlighted in black, which reduces the peak amplitude to 18% of the tuned case. The corresponding mistuning distribution is shown in the top left of the figure.

Keeping $\ell = 11$ fixed, we explore the influence of the mistuning amplitude in Fig. 18. Unlike the wavenumber 2 pattern, this configuration benefits from higher mistuning levels. The peaks in the response move farther apart as the amplitude increases, with the right peaks shifting away from ω_1. At 5% mistuning, the amplification factor drops to 1.09. This trend is explained by the absence of nearby modes to the right of ω_1, reducing the potential for additional coupling.

This effect is also reflected in the sensitivity to random mistuning, shown in Fig. 19. At low intentional mistuning levels, the spread in peak amplitudes is about 38%, similar to the wavenumber 2 case. As the mistuning level increases, the maximum amplification decreases more gradually. Nevertheless, in contrast to the previous strategy, at 5% mistuning amplitude, the spread is significantly reduced to just 5%. Therefore, the wavenumber 1 strategy is particularly effective in minimizing sensitivity to random mistuning, as it shifts the dominant modes to a region with fewer neighboring modes and lower interaction potential.

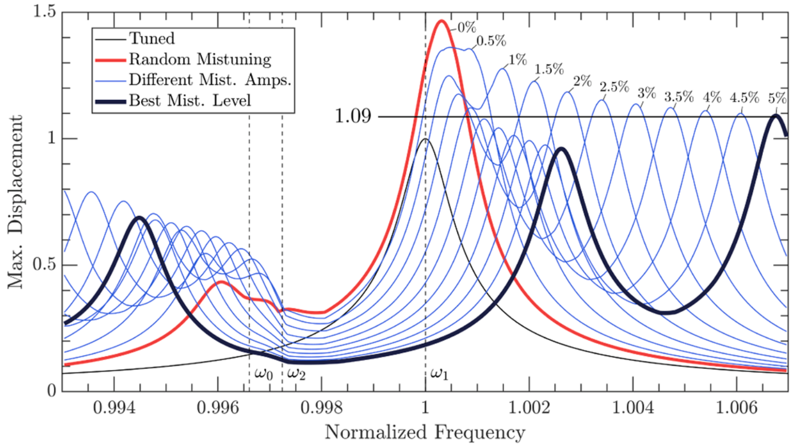

Fig. 18. Frequency response curve of the maximum displacements over all the sectors for different intentional mistuning amplitudes for the cosine pattern with wavenumber 1.

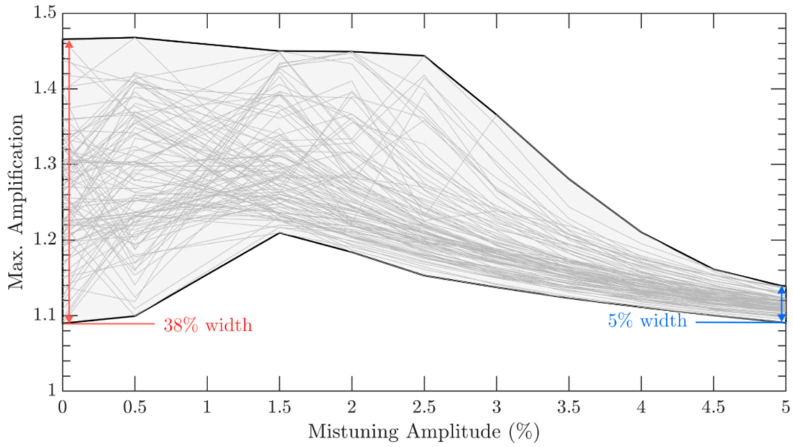

Fig. 19. Maximum amplification of all the random mistuning patterns in Fig. 9 for an intentional mistuning pattern with a cosine distribution of wavenumber 1.

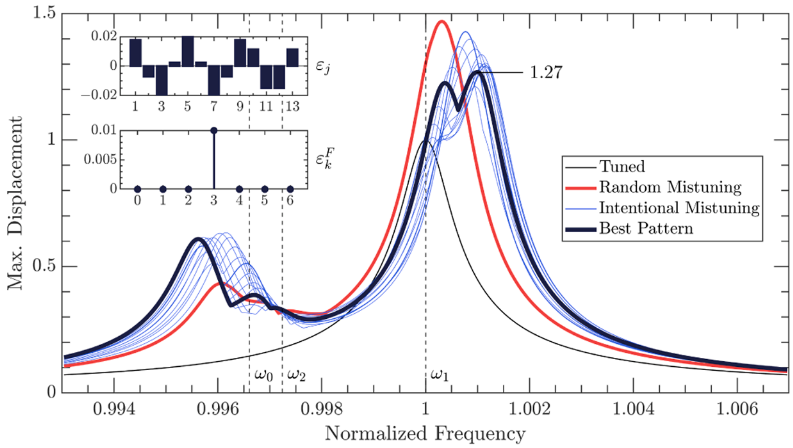

Fig. 20. Frequency response curve of the maximum displacement over all the sectors. Effect of the phase of the intentional mistuning pattern, $\varepsilon_j = 0.02 \cdot \cos((2\pi/N \cdot 3)(j-1) + (2\pi/N)\ell)$, for different ℓ. The lowest response is obtained for $\ell = 1$ (thick black line). Top left: intentional mistuning pattern with the highest reduction in physical space (ε_j), and in Fourier space (ε_k^F).

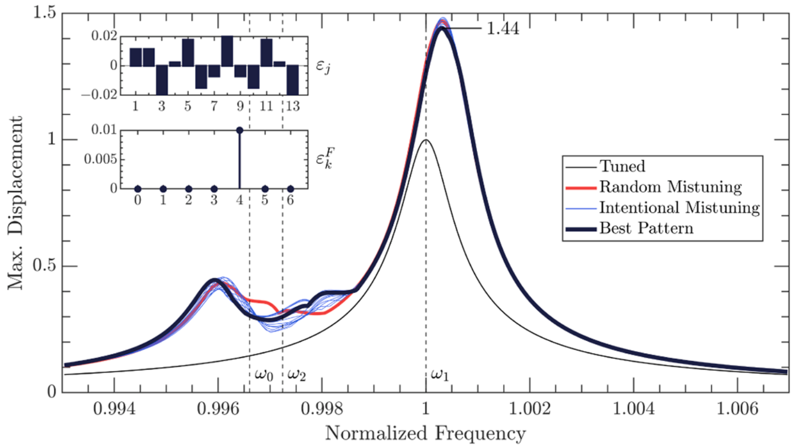

Fig. 21. Frequency response curve of the maximum displacement over all the sectors. Effect of the phase of the intentional mistuning pattern, $\varepsilon_j = 0.02 \cdot \cos((2\pi/N \cdot 4)(j-1) + (2\pi/N)\ell)$, for different ℓ. The lowest response is obtained for $\ell = 1$ (thick black line). Top left: intentional mistuning pattern with the highest reduction in physical space (ε_j), and in Fourier space (ε_k^F).

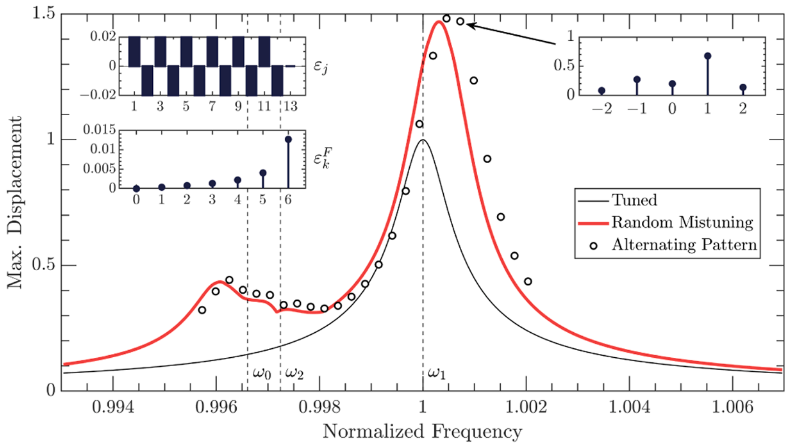

Fig. 22. Frequency response curve of the maximum displacement over all the sectors with an alternating mistuning pattern. The response is directly computed the full-order FEM model (dots). Top left: intentional mistuning pattern with the highest reduction in physical space (ε_j), and in Fourier space (ε_k^F). Top right: Modal amplitudes of the traveling waves $-2, -1, 0, 1, 2$ at the peak.

(c) Cosine pattern with wavenumber 3

In this case, we only evaluate the effect of the intentional mistuning pattern on the random configuration that produced the highest amplification, since the AMM predicts a limited impact compared to the previous strategies. The mistuning distribution is given by

$$\varepsilon_j \sim \cos((2\pi/N \cdot 3)(j-1) + (2\pi/N)\ell). \tag{31}$$

Fig. 20 shows the resulting frequency response curves for a 2% intentional mistuning level. The smallest amplification factor obtained is 1.27. Compared to the results in Figs. 13 and 17, it is evident that this mistuning pattern has a weaker influence on the response, making it less suitable for reducing the forced response.

(d) Cosine pattern with wavenumber 4

The mistuning pattern is defined as

$$\varepsilon_j \sim \cos((2\pi/N \cdot 4)(j-1) + (2\pi/N)\ell). \tag{32}$$

The frequency response curves for the different values of ℓ are shown in Fig. 21. As predicted by the AMM equations (Fig. 11), the Fourier component ε_4^F has a limited effect, coupling only modes 2 and -2. Consequently, the maximum response remains nearly unchanged across all shifts of the mistuning distribution. Some variation is observed in the left part of the plot, where modes 2 and -2 exhibit slight separation. Based on the AMM framework, it is evident that this mistuning pattern is ineffective in reducing the response (an outcome that can be anticipated without performing full numerical analysis).

(d) Alternating pattern

In the analysis of bladed-disks, alternating patterns have been widely used to reduce the forced response. For flat modal families, this type of mistuning splits the modes into two distinct groups, causing even and odd blades to vibrate at different frequencies, reducing their coupling and, thus, the amplification [28]. For the analysis of bladed-disks an additional assumption is typically made: the in-sector mode shapes for a flat family are identical, resulting in a simplification of the AMM Eq. (24).

Nevertheless, the situation for a centrifugal impeller differs substantially. The modes are not organized into a flat family, and the in-sector mode shapes of the active modes contributing to the response may differ significantly. The AMM equations derived for this case indicate that only $\Delta\mathbf{M}_1^F, \ldots, \Delta\mathbf{M}_4^F$ significantly influence the response (see Fig. 11). If the impeller had an even number of blades, such as 14, an alternating pattern would only produce a contribution at $\Delta\mathbf{M}_7^F$, which, according to the AMM, would have negligible impact on the forced response. In the present case, the blade count is odd ($N = 13$), and the alternating pattern does not exactly fit. The configuration considered assigns zero mistuning mass to one blade, as illustrated in the top left of Fig. 22. The Fourier decomposition of the mistuning pattern has a dominant component at $k = 6$, with contributions from other harmonics. Although some relevant Fourier components are present, their effect is expected to be limited due to their small size.

To confirm this, the alternating pattern is evaluated directly using the full FEM model, and the resulting resonance curve is shown in Fig. 22. The response is nearly identical to that of the case without intentional mistuning, and the modal content at the peak (top right of the figure) closely resembles the response associated with the random mistuning pattern in Fig. 9.

5. Conclusion

This study investigates the amplification of the forced response in a centrifugal impeller due to random mistuning and proposes practical strategies for mitigating this effect through intentional mistuning. The applied forcing excites a mode characterized by localized motion at the tips of the different sectors, corresponding to a crossing in the SAFE diagram, which is particularly dangerous due to high cycle fatigue.

We use the Asymptotic Mistuning Model (AMM), a drastically reduced but accurate description of the impeller forced response. This model captures the main physical mechanisms that govern the response, in particular the coupling mechanism of the modes through the Fourier coefficients of the sector-to-sector mistuning distribution. This insight guides the selection process of the effective intentional mistuning patterns, without necessarily requiring expensive optimization processes over an exponentially large number of configurations.

The AMM is validated against full FEM computations of a realistic centrifugal impeller. Subsequently, the amplification of the response of the system due to random mistuning is investigated in the simplified AMM setup, and intentional mistuning patterns are designed to reduce the amplification. The main contributions of this work can be summarized as follows:

1. For the frequency distribution of the centrifugal impeller analyzed in this study, an AMM model retaining only five active modes (five linear equations) accurately captures the forced response. The validations against full FEM simulations are done across several mistuning patterns, with a good prediction of the mistuned frequencies and differences less than 3% in the maximum amplitude.
2. A random mistuning distribution involving only 0.5% variation in sector mass can increase the response amplitude by up to 50% for localized tip modes in the configuration under analysis.
3. The AMM provides physical insight that guides the design of intentional mistuning patterns: modal coupling is governed by specific Fourier coefficients of the sector-to-sector mistuning distribution. Once the modes that actively participate in the mistuned response are identified, the corresponding intentional mistuning pattern can be designed directly from the structure of the AMM equations.
4. The mistuned frequencies and mode shapes can be accurately predicted by solving the reduced eigenvalue problem defined by the AMM equations, which involves only the active modes.
5. In particular, in the study of the mistuned forced response of a mode with tip-localized motion and wavenumber 1, the dominant response involves TWs $0, \pm 1, \pm 2$. The most effective intentional mistuning patterns in this case are cosine distributions with wavenumber 2 (to separate TWs 1 and -1) or wavenumber 1 (to decouple neighboring modes), in agreement with the AMM predictions.
6. The arrangement of the intentional mistuning pattern along the impeller is relevant. For a configuration with 13 sectors, shifting the pattern by multiples of the interblade phase angle results in different forced response outcomes.
7. For the analyzed impeller, the amplification can be reduced to within 1% of the tuned response using an appropriately designed intentional mistuning pattern.
8. Sensitivity to random mistuning is reduced when intentional mistuning shifts the dominant modes in the response away from nearby frequencies.
9. Intentional mistuning patterns that contain no relevant Fourier components of the sector-to-sector mistuning distribution produce negligible changes in the response.
10. Alternating intentional mistuning patterns, typically used in bladed-disk configurations, are ineffective for centrifugal impellers with a modal distribution similar to the one presented in Fig. 3a. In the former case, this pattern is effective because the modal families are flat and well-separated from each other, splitting the modes into two distinct groups with much lower coupling. The mode distribution of the impeller is fundamentally different, and the alternating pattern does not result in a significant reduction in the response.

CRediT authorship contribution statement

Giulio Deiana: Writing – review & editing, Writing – original draft, Visualization, Validation, Software, Methodology, Investigation, Formal analysis; **Javier González-Monge:** Writing – review & editing, Writing – original draft, Visualization, Validation, Supervision, Software, Methodology, Investigation, Formal analysis, Conceptualization; **Carlos Martel:** Writing – review & editing, Writing – original draft, Visualization, Validation, Supervision, Methodology, Investigation, Formal analysis, Conceptualization; **Alberto Guglielmo:** Supervision; **Giulio Costa:** Supervision; **Enrico Meli:** Funding acquisition, Supervision.

Data availability

The data that has been used is confidential.

Declaration of competing interest

The authors declare that they have no known competing financial interests or personal relationships that could have appeared to influence the work reported in this paper.

Acknowledgment

The authors gratefully acknowledge the company Baker Hughes for its support and fruitful collaboration throughout this research activity.

References

[1] M.P. Castanier, C. Pierre, Modeling and analysis of mistuned bladed disk vibration: current status and emerging directions, J. Propuls. Power 22 (2) (2006) 384–396. https://doi.org/10.2514/1.16345
[2] R. Bladh, M.P. Castanier, C. Pierre, Reduced order modeling and vibration analysis of mistuned bladed disk assemblies with shrouds, J. Eng. Gas Turbines Power 121 (3) (1999) 515–522. https://doi.org/10.1115/1.2818503
[3] R. Bladh, M.P. Castanier, C. Pierre, Component-mode-based reduced order modeling techniques for mistuned bladed disks-Part I: theoretical models, J. Eng. Gas Turbines Power 123 (1) (2000) 89–99. https://doi.org/10.1115/1.1338947
[4] P. Vargiu, C.M. Firrone, S. Zucca, M.M. Gola, A reduced order model based on sector mistuning for the dynamic analysis of mistuned bladed disks, Int. J. Mech. Sci. 53 (8) (2011) 639–646. https://doi.org/10.1016/j.ijmecsci.2011.05.010
[5] M.-T. Yang, J.H. Griffin, A reduced-order model of mistuning using a subset of nominal system modes, J. Eng. Gas Turbines Power 123 (4) (1999) 893–900. https://doi.org/10.1115/1.1385197
[6] A. Sinha, Reduced-order model of a bladed rotor with geometric mistuning, J. Turbomach. 131 (3) (2009) 031007. https://doi.org/10.1115/1.2987237
[7] Y. Bhartiya, A. Sinha, Reduced order modeling of a bladed rotor with geometric mistuning via estimated deviations in mass and stiffness matrices, J. Eng. Gas Turbines Power 135 (5) (2013) 052501. https://doi.org/10.1115/1.4007783
[8] D.M. Feiner, J.H. Griffin, A fundamental model of mistuning for a single family of modes, J. Turbomach. 124 (4) (2002) 597–605. https://doi.org/10.1115/1.1508384
[9] D.M. Feiner, J.H. Griffin, Mistuning identification of bladed disks using a fundamental mistuning model-Part I: theory, J. Turbomach. 126 (1) (2004) 150–158. https://doi.org/10.1115/1.1643913
[10] D.M. Feiner, J.H. Griffin, Mistuning identification of bladed disks using a fundamental mistuning model-Part II: application, J. Turbomach. 126 (1) (2004) 159–165. https://doi.org/10.1115/1.1643914
[11] C. Martel, R. Corral, Asymptotic description of maximum mistuning amplification of bladed disk forced response, J. Eng. Gas Turbines Power 131 (2) (2008) 022506. https://doi.org/10.1115/1.2968868
[12] O. Khemiri, C. Martel, R. Corral, Asymptotic description of damping mistuning effects on the forced response of turbomachinery bladed disks, J. Sound Vib. 332 (20) (2013) 4998–5013. https://doi.org/10.1016/j.jsv.2013.04.030
[13] O. Khemiri, C. Martel, R. Corral, Forced response of mistuned bladed disks: quantitative validation of the asymptotic description, J. Propuls. Power 30 (2) (2014) 397–406. https://doi.org/10.2514/1.B34631
[14] D.S. Whitehead, Effect of mistuning on the vibration of turbo-machine blades induced by wakes, J. Mech. Eng. Sci. 8 (1) (1966) 15–21. https://doi.org/10.1243/JMES_JOUR_1966_008_004_02
[15] D.S. Whitehead, The maximum factor by which forced vibration of blades can increase due to mistuning, J. Eng. Gas Turbines Power 120 (1) (1998) 115–119. https://doi.org/10.1115/1.2818061
[16] A. Sinha, Computation of the maximum amplitude of a mistuned bladed disk assembly via infinity norm Analysis and Design Issues for Modern Aerospace Vehicles (1997) 427–432. https://doi.org/10.1115/IMECE1997-0742
[17] A.J. Rivas-Guerra, M.P. Mignolet, Maximum amplification of blade response due to mistuning: localization and mode shape aspects of the worst disks, J. Turbomach. 125 (3) (2003) 442–454. https://doi.org/10.1115/1.1506958
[18] A. Sinha, Vibration of Nearly Periodic Structures and Mistuned Bladed Rotors, Cambridge University Press, 2017. https://doi.org/10.1017/9781316986806
[19] A. Sinha, Solving fundamental partial differential equation for mistuned bladed disk vibration, AIAA J. 60 (6) (2022) 3931–3935. https://doi.org/10.2514/1.J061150
[20] M.P. Mignolet, W. Hu, I. Jadic, On the forced response of harmonically and partially mistuned bladed disks. Part I: harmonic mistuning, Int. J. Rotating Mach. 6 (1) (2000) 926815. https://doi.org/10.1155/S1023621X0000004X
[21] J.A. Kenyon, J.H. Griffin, Forced response of turbine engine bladed disks and sensitivity to harmonic mistuning, J. Eng. Gas Turbines Power 125 (1) (2002) 113–120. https://doi.org/10.1115/1.1498269
[22] L. Pohle, L. Panning-von Scheidt, J. Wallaschek, Harmonic mistuning of blisks, PAMM 15 (1) (2015) 641–642. https://doi.org/10.1002/pamm.201510310
[23] S. Willeke, L. Schwerdt, L. Panning-von Scheidt, J. Wallaschek, Intentional response reduction by harmonic mistuning of bladed disks with aerodynamic damping, J. Eng. Gas Turbines Power 140 (12) (2018) 121010. https://doi.org/10.1115/1.4040898
[24] G. Deiana, G. Costa, A. Guglielmo, E. Meli, New modal tracking methods for cyclic structures - application to centrifugal compressor impellers, in: Proceedings of ASME Turbo Expo 2025: Turbomachinery Technical Conference and Exposition, ASME, Memphis, Tennessee, 2025, pp. GT2025–151263.
[25] M.P. Castanier, C. Pierre, Using intentional mistuning in the design of turbomachinery rotors, AIAA J. 40 (10) (2002) 2077–2086. https://doi.org/10.2514/2.1542
[26] B.-K. Choi, J. Lentz, A.J. Rivas-Guerra, M.P. Mignolet, Optimization of intentional mistuning patterns for the reduction of the forced response effects of unintentional mistuning: formulation and assessment, J. Eng. Gas Turbines Power 125 (1) (2002) 131–140. https://doi.org/10.1115/1.1498270

[27] Y. Han, R. Murthy, M.P. Mignolet, J. Lentz, Optimization of intentional mistuning patterns for the mitigation of the effects of random mistuning, J. Eng. Gas Turbines Power 136 (6) (2014) 062505. https://doi.org/10.1115/1.4026141
[28] J.J. Sánchez-Álvarez, C. Martel, Key action mechanisms of intentional mistuning, Appl. Sci. 11 (12) (2021). https://doi.org/10.3390/app11125650
[29] C. Martel, R. Corral, J.M. Llorens, Stability increase of aerodynamically unstable rotors using intentional mistuning, J. Turbomach. 130 (1) (2007) 011006. https://doi.org/10.1115/1.2720503
[30] R. Corral, O. Khemiri, C. Martel, Design of mistuning patterns to control the vibration amplitude of unstable rotor blades, Aerosp. Sci. Technol. 80 (2018) 20–28. https://doi.org/10.1016/j.ast.2018.06.034
[31] C. Martel, J.J. Sánchez-Álvarez, Intentional mistuning effect in the forced response of rotors with aerodynamic damping, J. Sound Vib. 433 (2018) 212–229. https://doi.org/10.1016/j.jsv.2018.07.020
[32] E.P. Petrov, Reduction of forced response levels for bladed disks by mistuning: overview of the phenomenon, J. Eng. Gas Turbines Power 133 (7) (2011) 072501. https://doi.org/10.1115/1.4002619
[33] B. Beirow, F. Figaschewsky, A. Kühhorn, A. Bornhorn, Vibration analysis of an axial turbine blisk with optimized intentional mistuning pattern, J. Sound Vib. 442 (2019) 11–27. https://doi.org/10.1016/j.jsv.2018.10.064
[34] B. Beirow, A. Nakos, M. Golze, D. Vogt, M. Wirsum, M. Schafferus, M. Sasakaros, Forced response reduction of a turbine impeller, in: Advances in Mechanism Design IV, Springer Nature Switzerland, 2024, pp. 53–65. https://doi.org/10.1007/978-3-031-70251-8_6
[35] B. Beirow, A. Nakos, C. Stecklina, M. Noack, M. Firl, M. Sasakaros, Implementation of intentional mistuning by means of finite element-based shape optimization, J. Eng. Gas Turbines Power 148 (4) (2025) 041003. https://doi.org/10.1115/1.4069624
[36] B.C. Pettinato, Y. Wang, J.H. Griffin, D.M. Feiner, B. Echols, M. Cushman, Experimentally based statistical forced response analysis for purpose of impeller mistuning identification, in: Proceedings of the Second Middle East Turbomachinery Symposium, 17–20 March 2012, Doha, Qatar, Turbomachinery Laboratory, Texas A&M University, College Station, TX, 1–12 (2013), https://hdl.handle.net/1969.1/172623.
[37] S. Wang, Y. Zi, B. Li, C. Zhang, Z. He, Reduced-order modeling for mistuned centrifugal impellers with crack damages, J. Sound Vib. 333 (25) (2014) 6979–6995. https://doi.org/10.1016/j.jsv.2014.07.009
[38] X. Zhao, H. Li, S. Yang, Z. Fan, J. Dong, H. Cao, Blade vibration measurement and numerical analysis of a mistuned industrial impeller in a single-stage centrifugal compressor, J. Sound Vib. 501 (2021) 116068. https://doi.org/10.1016/j.jsv.2021.116068
[39] F. Moyroud, S. Livet, J. Jiang, R. Sampath, Semi-automatic mode naming methodology to classify impeller mode families, 10th International Conference on Vibrations in Rotating Machinery, Woodhead Publishing 2012, pp. 199–210. ISBN 978-0-85709-452-0 https://doi.org/10.1533/9780857094537.4.199
[40] M. Singh, History of evolution, progress and application of SAFE diagram for tuned and mistuned systems, in: Proceedings of the Forty-Second Turbomachinery Symposium, October 1–3, 2013, Houston, Texas, Texas A&M University. Turbomachinery Laboratories, 1–31 (2013), https://hdl.handle.net/1969.1/162911.
[41] O. Schenk, K. Gärtner, W. Fichtner, A. Stricker, PARDISO: a high-performance serial and parallel sparse linear solver in semiconductor device simulation, Future Gener. Comput. Syst. 18 (1) (2001) 69–78. https://doi.org/10.1016/S0167-739X(00)00076-5